Journal of Biomedical Optics

SPIEDigitalLibrary.org/jbo

Optical coherence tomography microangiography for monitoring the response of vascular perfusion to external pressure on human skin tissue

Woo June Choi
Hequn Wang
Ruikang K. Wang

Optical coherence tomography microangiography for monitoring the response of vascular perfusion to external pressure on human skin tissue

Woo June Choi, Hequn Wang, and Ruikang K. Wang*
University of Washington, Department of Bioengineering, Seattle, Washington 98195

Abstract. Characterization of the relationship between external pressure and blood flow is important in the examination of pressure-induced disturbance in tissue microcirculation. Optical coherence tomography (OCT)-based microangiography is a promising imaging technique, capable of providing the noninvasive extraction of functional vessels within the skin tissue with capillary-scale resolution. Here, we present a feasibility study of OCT microangiography (OMAG) to evaluate changes in blood perfusion in response to externally applied pressure on human skin tissue *in vivo*. External force is loaded normal to the tissue surface at the nailfold region of a healthy human volunteer. An incremental force is applied step by step and then followed by an immediate release. Skin perfusion events including baseline are continuously imaged by OMAG, allowing for visualization and quantification of the capillary perfusion in the nailfold tissue. The tissue strain maps are simultaneously evaluated through the available OCT structural images to assess the relationship of the microcirculation response to the applied pressure. The results indicate that the perfusion progressively decreases with the constant increase of pressure. Reactive hyperemia occurs right after the removal of the pressure. The perfusion returns to the baseline level after a few minutes. These findings suggest that OMAG may have great potential for quantitatively assessing tissue microcirculation in the locally pressed tissue *in vivo*. [DOI: 10.1117/1.JBO.19.5.056003]

Keywords: optical coherence tomography; optical microangiography; skin vascular perfusion; external pressure.

Paper 140159R received Mar. 8, 2014; revised manuscript received Apr. 13, 2014; accepted for publication Apr. 16, 2014; published online May 8, 2014.

1 Introduction

Over the last decades, there has been growing interest in cutaneous microcirculation response to external pressure.[1–5] Change in the skin blood flow against pressure has been clinically considered as an important indicator to assess microcirculatory disorder in vascular disease related to diabetic mellitus (DM)[2,3] or development of pressure ulcers as complications related to the care and treatment of primarily disabled and elderly people.[4] Therefore, the characterization of the external pressure-flow relationship is essential for understanding vascular hemodynamics in the pressed tissue. Few optical techniques have been employed for investigating the pressure-flow relationship in a noninvasive and reproducible manner. Laser Doppler flowmetry (LDF) is one of the most prevalently used techniques in the skin perfusion study.[2–5] It is based on the well-known Doppler frequency shifts of lights scattered by moving red blood cells (RBCs) in the vessels upon laser illumination.[6] However, it only provides the measurement of blood flow at a single point on the tissue. Recently, two-dimensional (2-D) image sensor-based laser Doppler imaging (LDI) techniques have shown the possibility to extend the point measurement of LDF into *en face* perfusion imaging for the skin tissue.[7,8] Despite real-time *in vivo* assessment of the blood flow in the skin tissue, their use is limited to estimate the overall level of the skin perfusion due to their limited resolution, which is insufficient to explore substantial flow events generated by vasculatures consisting of small vessels (arterioles and venules) or capillaries. In addition, they are unable to provide the depth-resolved vasculature image. Currently, what is preferred is an imaging technique that can provide three-dimensional (3-D) microvasculature imaging at the capillary level for evaluating the detailed flow dynamics of microvessel network within skin tissue under pressure.

Optical coherence tomography (OCT) is a noninvasive optical imaging modality, capable of providing 3-D tomographic images of living tissues with micrometer resolution.[9,10] Recently, the functional utilization of OCT has enabled extracting depth-resolved blood perfusion maps within tissue beds *in vivo*.[11–13] Vascular contrast in OCT is sourced from the dynamic scattering property of moving RBCs in the vessel lumen, which can be differentiated from the static scattering of the stationary tissues surrounding the vessels.[11] This endogenous vascular mapping is beneficial for tissue viability compared to conventional angiographic methods using exogenous contrast agents causing possible adverse effects.[14] Several OCT microangiography (OMAG) techniques have been proposed and developed, including methods based on phase variation [e.g., phase-variance OCT (Ref. 15)], intensity variation [e.g., speckle variance OCT (svOCT)[16] and correlation mapping OCT (cmOCT)[17]], and complex signal variation [ultrahigh sensitive OMAG (UHS-OMAG)[18,19]] in the OCT signal. Many vascular works using these methods have demonstrated an ability to delineate microcirculation in a wide variety of microcirculatory tissue beds such as brain,[11–13] eye,[15,19–21]], skin[16–18] in humans as well as small animals *in vivo*.

*Address all correspondence to: Ruikang K. Wang, E-mail: wangrk@uw.edu

0091-3286/2014/$25.00 © 2014 SPIE

The aim of this study is to demonstrate the capability of OMAG in the investigation of the effect of externally applied pressure on skin vascular perfusion. The 3-D microvascular imaging of this microangiographic technique can offer both qualitative and quantitative information as to the response of blood flow within a highly localized region to the different levels of pressure applied. The utility of the OMAG for studying the pressure-flow relationship has been reported for retina of anesthetized small animals *in vivo*,[22] but no report, to the best of our knowledge, has so far demonstrated its feasibility for the study of the human skin tissue *in vivo*.

2 Materials and Methods

2.1 *Imaging System*

In this study, we used a fiber-based swept source OCT (SS-OCT) system consisting of a Mach-Zehnder interferometer and a balanced detector. The overall specification of the system is described in our previous work.[23] Briefly, a swept laser source (VCSEL laser, Thorlabs, Newton, New Jersey) having a central wavelength of 1300 nm with a 100 nm bandwidth at 10 dB cut-off point was employed in the system, producing an axial resolution of ~12 μm in water. The sample arm incorporated a stand-alone probe head containing X-Y galvo scanners, a collimator and a microscope objective (LSM03, 5× magnification, Thorlabs) mounted on the probe head [Fig. 1(a)]. A plastic plate with a 25-mm diameter hole was affixed to the probe head using movable space bars to enable adjustment in distance between the objective and the plate. A 1-mm thick flat glass slide (optical transmission: >90% at 1300 nm) was attached to the plastic plate using double-sided tape and was in contact with the skin surface, which allowed for applying pressure normal to the skin surface during OCT imaging. In this work, the nailfold region was chosen as the tissue site for imaging under pressure because that the region contains well-defined capillary structures parallel to the skin surface, which, however, appears perpendicular to other skin sites.[24,25] The parallel arrangement of microvascular appearance may permit observation of significant flow change in the skin capillary when being pressed. Particularly, the nailfold of the fourth finger was tested to achieve the best visibility because of greater transparency than those of other fingers.[25] The fingertip was placed under the probe head and the top surface of the nailfold was carefully positioned in parallel to the glass slide for uniform pressing across the surface area. The fingertip was then stabilized with supporting clay to reduce artifacts caused by involuntary body movement. Ultrasound gel was applied between the nailfold surface and the glass slide as a coupling material to mitigate the refractive index difference.[26] The probing beam from the OCT system was incident upon the nailfold surface through the glass slide with an average optical power of ~3.2 mW and was focused into the skin [Fig. 1(b)]. Such a sample preparation makes the working distance become 500 μm longer than the nominal one (25.1 mm in air) due to the presence of the glass (average RI: 1.5). The lateral resolution was measured to be 25 μm.

The A-scan rate of the system was fixed to 100,000 lines/s, with which the system sensitivity was estimated to be 103 dB at the focus spot of the probing beam. The OCT data acquisition was achieved by the X-Y galvo scanning in which the scanning probe beam was tracked with a red laser that was used as an aiming beam. The scan resulted in one volumetric OCT data over the scanned tissue area. From the obtained 3-D data cube, both the tissue structure and corresponding vasculature were extracted simultaneously.

2.2 *Data Acquisition and Processing*

For 3-D vascular imaging of the skin tissue with the system, we adopted a scanning protocol of UHS-OMAG in which the 3-D tissue perfusion maps have been successfully achieved with a flow sensitivity down to a capillary perfusion level.[18] In this protocol, the raster scanning was performed to record a B-frame (XZ cross-sectional image) with 256 A-lines for fast B-scan (in X-direction) and 2560 cross sections for slow C-scan (in Y-direction). This means that the completed scanning produces a 3-D volume data containing $256\,(X) \times 2560\,(Y) \times 4096\,(Z)$ voxels, where 4096 is a sampling pixel number in one A-line. Using the B-frame imaging speed of 100 frames/s (fps), we were able to acquire the 3-D OCT data cube in ~26 s. Considering a scan region of 2 mm $(X) \times 2$ mm (Y), spatial gaps between adjacent A-lines and inter-B-frames were 7.8 and 0.78 μm, respectively. Because phase measurement is challenging to the SS-OCT system due to sampling or A-scan trigger jitter,[27] the flow image processing was conducted with amplitudes of the obtained OCT raw data, calculated after fast Fourier transform of the

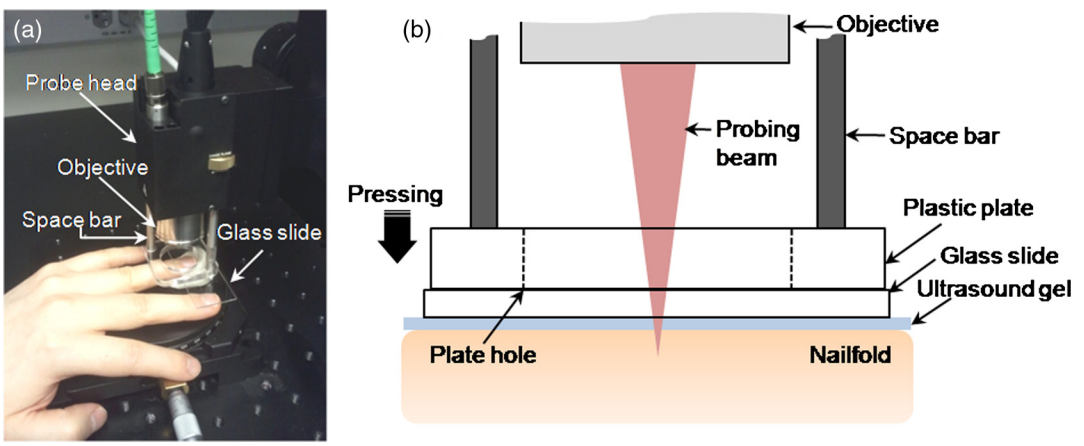

Fig. 1 (a) Photograph of the probe head in the sample arm of the swept source optical coherence tomography (OCT) system and (b) the schematic of the probe head-skin interface.

complex OCT signals. One cross-sectional flow intensity image was extracted from the absolute difference between the subsequent amplitude B-frames as follows:

$$I_{\text{flow}}(i) = |I(i+1) - I(i)|, \tag{1}$$

where $I(i)$ is a i'th amplitude B-frame and $I_{\text{flow}}(i)$ is a i'th flow intensity image. This differential operation serves as high-pass filtering, allowing suppression of the optical scattering signals from the static tissues, which is quite similar to the data processing of UHS-OMAG, where the complex form of the OCT signals was, however, used.[18] To increase the sensitivity of the flow signal, nine flow intensity images calculated from 10 consecutive amplitude B-frames were averaged. Since the sum of the spatial gaps between the 10 consecutive amplitude B-frames is ~7 μm, less than half of the system lateral resolution of 25 μm, it can be treated as though the nine flow intensity images were acquired at the same location. With all 256 cross-sectional flow intensity images, a 3-D vascular map was constructed.

Through the application of the high-pass filtering on the blood flow calculation, it was found that the scattering signals arising from the high reflective tissue structures still resulted in residuals on the vascular image, degrading the flow image quality. To reduce these artifacts, we carried out additional cmOCT imaging with the same OCT data set. The cmOCT image is based on amplitude correlation between inter-B-frames, which gives relative immunity to the artifacts from the high intensity structural regions compared to the UHS-OMAG.[28] Thus, a binary form (1: flow region, 0: flow-free region) of the cmOCT image was used as a mask on the UHS-OMAG image. By overlaying the cmOCT mask on the UHS-OMAG image, it can block the static signals from the flow distribution. Concept and process of this scheme are detailed in a recent paper.[28] As a result, the 256 cross-sectional UHS-OMAG images were masked with a corresponding binary cmOCT image, and the masked UHS-OMAG images (named mOMAG images) were displayed with a logarithmic scale. The post-data processing was performed with a laboratory-software coded by a MATLAB language (Ver. 7.6, MathWorks) on a personal laptop (2.9 GHz, 8 GB RAMS). Total processing time to obtain a resultant 3-D vascular map took about 15 min. One *en face* microangiogram was displayed by projecting voxels with maximum intensity values in the 3-D vasculature.

2.3 *Experimental Design*

In order to monitor skin blood flow response to the applied pressure, we performed microvascular imaging of human nailfold with the following experimental protocol; first, a healthy volunteer was in a seated position and allowed to adapt to the environment for 15 min at room temperature (23°C) before the measurement. A baseline measurement was conducted without any stress on the nailfold tissue with the glass slide almost just in touch with the skin surface. The load was then applied through the glass slide by manually moving the probe head forward to the nailfold with a step increment of 50 μm, which was

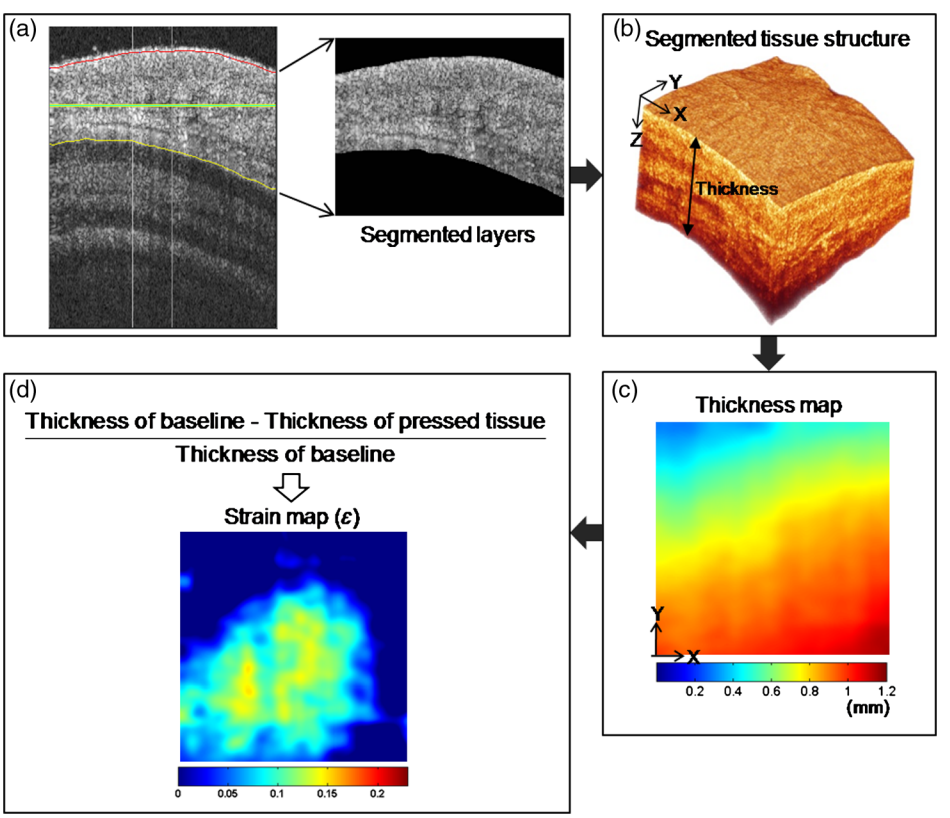

Fig. 2 Flow diagram of the procedure for strain calculation. (a) Segmentation of the tissue structure (between red and yellow lines) to be deformed from the cross-sectional OCT structural image of the nailfold, (b) segmented three-dimensional (3-D) tissue structure obtained from all OCT structural images of the nailfold, (c) *en face* thickness map calculated from the segmented 3-D tissue structure (b), and (d) corresponding *en face* strain map calculated using Eq. (3) with *en face* thickness maps obtained from baseline and each measurement with external loading.

monitored in real time through B-mode OCT imaging at 100 fps. Displacement of the glass slide ranged from 0 to 200 μm relative to its initial position, where 200 μm was an empirically set minimal displacement for complete obstruction of the capillary flow in the nailfold, meaning a total disappearance of the dynamic scattering within B-mode OCT imaging. For each displacement (took about 5 s), 3-D OCT imaging of the pressed nailfold was carried out for 26 s and followed by a rest time of 10 s. After that, the pressure was suddenly released by quickly moving the probing head backward and one OCT measurement was taken right after the pressure release. Then, two postpressure measurements were acquired with 1-min intervals. Subsequently, a total of eight measurements consisting of four sessions (prepressure (baseline), pressure application, pressure release, and postpressure) were taken within a time period of ~6 min.

2.4 *Quantification of Vascular Perfusion and External Pressure*

To characterize the pressure-flow relationship, it is necessary to quantify the vascular perfusion and the load distribution over the nailfold. In this work, the extent of vascular perfusion was represented as a flow index (FI), which can be defined as a ratio of perfusion area to total scanned area given by

$$\mathrm{FI} = \int_V \mathrm{d}a \Big/ \int_S \mathrm{d}a, \tag{2}$$

where V and S are the functional vessel area and the total scanned area on the mOMAG angiogram, respectively. The vessel area can be calculated by counting white pixels (with positive value of 1) from a binary form of the mOMAG angiogram. The FI values lie in the range [0, 1]. For the load distribution, it was very difficult to know the actual local pressure forced to the nailfold with the lack of a loading device to record the pressure. To circumvent this issue, we evaluated local strain proportional to the local pressure with the assumption that the pressure is applied along one axis (Z-axis here) to the uniform, isotropic, and incompressible tissue.[29] The strain ε is defined as an observed deformation relative to the initial state of the sample and can be expressed as fractional change in the thickness

$$\varepsilon = \frac{\Delta L}{L_0}, \tag{3}$$

where L_0 and ΔL are denoted as the initial thickness of the sample before stress and incremental (or decremental) change of the thickness after stress, respectively. This quantity would be useful as an alternative to estimate the local pressure on the tissue.

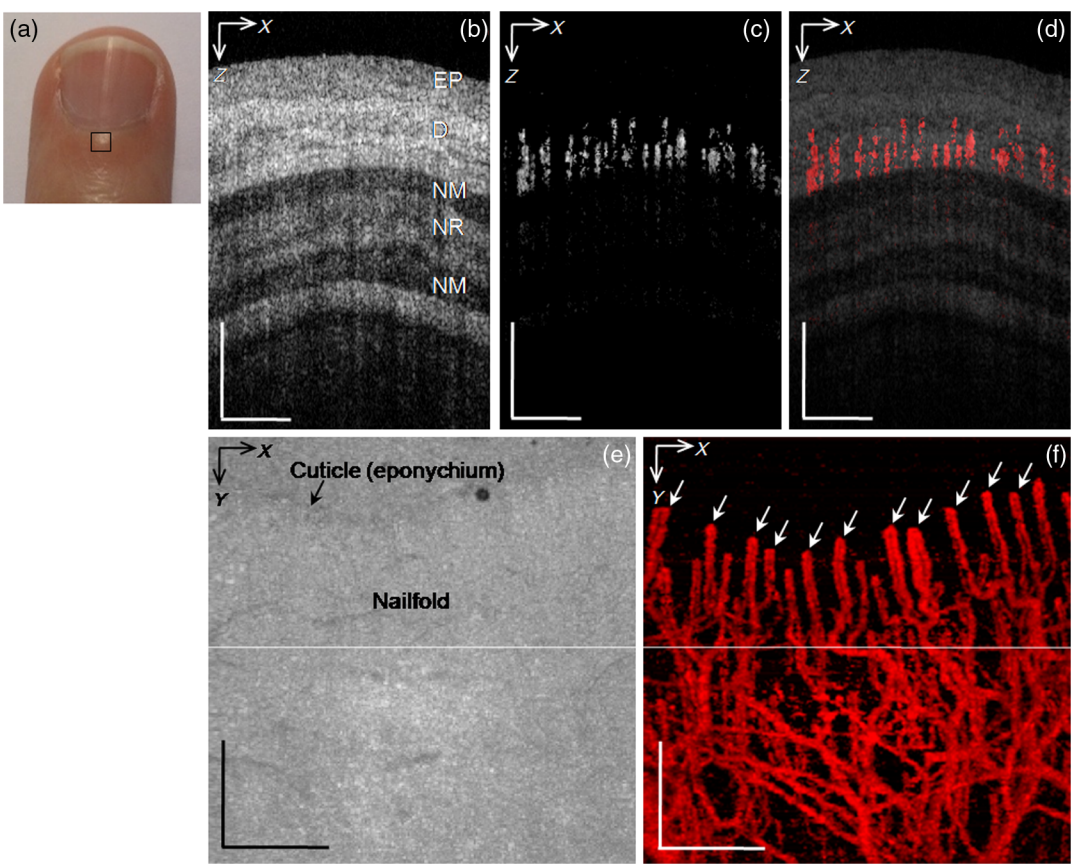

Fig. 3 *In vivo* microvascular imaging of a normal human nailfold with no pressure. (a) Photograph of a fourth finger of a left hand with an imaged area of the nailfold (a square box, 2 mm × 2 mm). (b) Representative cross-sectional (XZ) OCT structural image, EP: epidermis, D: dermis, NM: nail matrix, and NR: nail root. (c) Corresponding cross-sectional capillary flow image (mOMAG image). (d) The structural image of the nailfold with the color-coded (red) mOMAG image overlay. (e and f) *En face* (XY) maximum intensity projection (MIP) images of the nailfold structure and color-coded (red) vasculature from the same location, respectively. The horizontal white line on (e) and (f) indicates where the cross sections are shown in (b) and (c), respectively. Scale bars: 500 μm.

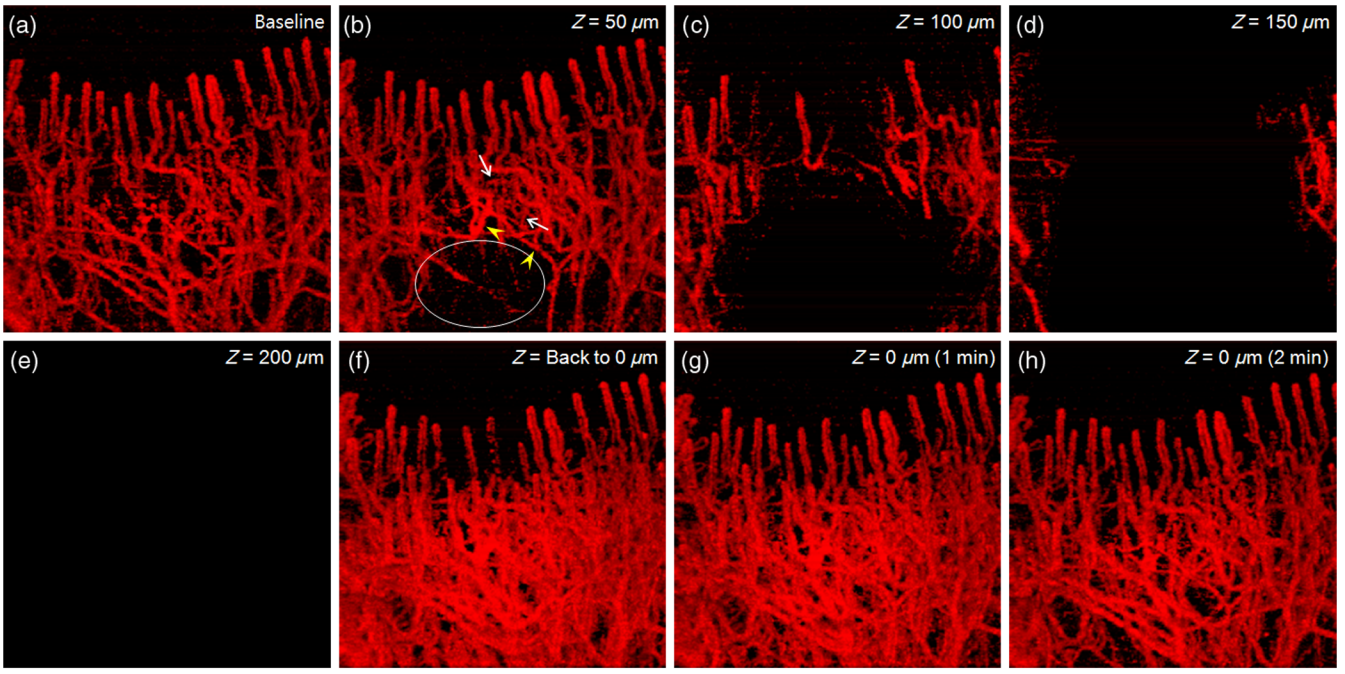

Fig. 4 *En face* capillary angiograms of the nailfold against the displacements from the initial position of the glass slide in contact to the nailfold surface. (a) Baseline, (b) $Z = 50$ μm, (c) $Z = 100$ μm, (d) $Z = 150$ μm, (e) $Z = 200$ μm, (f) $Z =$ back to 0 μm, (g) $Z = 0$ μm (1 min after pressure releasing), and (h) $Z = 0$ μm (2 min after pressure releasing). In the initial loading (b), cessation of local capillary perfusion is observed (white circle). Perfusion in other vessels close to the ceased capillaries is increased (arrow heads) allowing reserved capillary recruitments (arrows). A scale bar: 500 μm.

To measure the strain, a tissue segmentation algorithm developed by our group was used to calculate the thickness of the deformed tissue structure in the nailfold from the OCT cross-sectional structural images.[30] In this method, the structure between the tissue surface subject to the pressure and the specific inner layer insensitive relative to the pressure in the nailfold was segmented by semiautomatically tracking the target tissue layers on the OCT image.[30] As this process was applied to all OCT cross sections, a 3-D tissue structure was segmented. Thickness of the segmented structure was calculated and thus a 2-D thickness map was created. Because the loading may cause tissue displacement in the lateral direction, it may change tissue location. To mitigate this problem, position alignment between the thickness maps obtained from each measurement was carefully taken prior to the strain calculation, which may result in a slight downsizing of the thickness maps. Finally, a total of eight strain maps were calculated with the eight corrected thickness maps using Eq. (3). Figure 2 illustrates a flow diagram of the procedure to calculate the local strain.

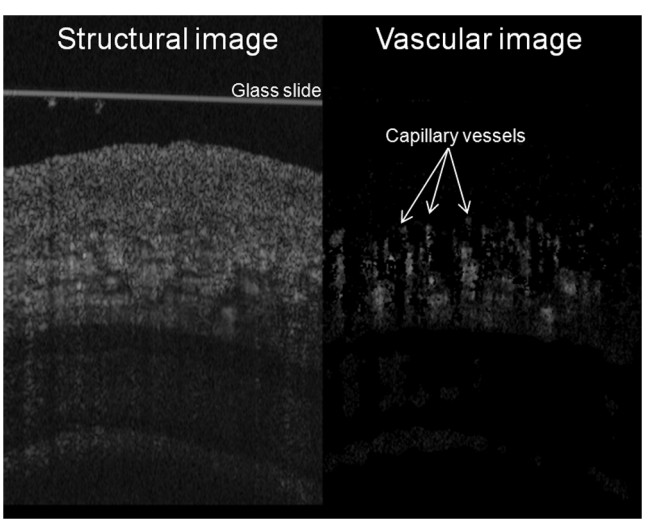

Fig. 5 Representative OCT structural image and corresponding vascular image excerpted from the animation showing time-lapsed change in structure and vasculature of the human nailfold with consecutive pre/postloading process (MPEG, 4.5 MB) [URL: http://dx.doi.org/10.1117/1.JBO.19.5.056003.1].

3 Experimental Results

3.1 *Microvascular Imaging of Human Nailfold*

Figure 3 shows *in vivo* microvascular imaging of the nailfold with no pressure (baseline) where the imaged area (2 mm × 2 mm) is marked as a square box in a photograph of the fourth finger of the left hand [Fig. 3(a)]. In Fig. 3(b), a representative *XZ* cross-sectional OCT image exhibits structural features in the nailfold such as epidermis (E), dermis (D), nail root (NR), and nail matrix (NM). In the corresponding cross-sectional mOMAG image [Fig. 3(c)], many bright signals are visible, representing blood perfusion in the capillaries. The structure image with the false colored (red) mOMAG overlay identifies the capillary flow in the dermal layer (D) as shown in Fig. 3(d). Maximum intensity projection (MIP) views were made with the structure and the vasculature, and the results are shown in Figs. 3(e) and 3(f), respectively. In Fig. 3(f), regular disposition of the hair pin-like capillary loops (arrows) along

the cuticle (eponychium) is clearly seen, a typical characteristic pattern of the nailfold capillary for the healthy subject.[25]

3.2 *Microvascular Imaging of Human Nailfold with Graded External Pressure*

The capillary perfusion change against the displacements of the glass slide is presented in Fig. 4 with the *en face* angiograms captured from each measurement. At displacement of $Z = 50$ μm [Fig. 4(b)], the signal loss is observed in the middle of the proximal region from the capillary loops (indicated by the white circle) compared to the baseline [Fig. 4(a)], suggesting that the blood flow was ceased due to the obstruction of the vessel under the pressed tissue structure. Qualitatively, it is noted that there is an increase in capillary flow (arrow heads) and new appearance of capillaries (arrows) after loading was applied [Fig. 4(b)]. It can be explained that the blood flow was detoured to different intact vessels close to the obstructed vessels, leading to flow increase in the detoured vessels, meaning that the reserve capillaries are recruited. In normal tissue state, the reserve vessels are in existence but with no or minimum blood flow.[31] However, the greater the displacements of the glass slide from 100 to 150 μm, the larger the vessel area is occluded. This is shown in Figs. 4(c) and 4(d), followed by complete occlusion across the whole capillary network at $Z = 200$ μm [Fig. 4(e)]. On releasing the occlusion, the mOMAG angiogram in Fig. 4(f) shows remarkable increase in the capillary reperfusion over the preocclusion (baseline), indicative of reactive hyperemia.[4] This hemodynamic behavior may be due to vasodilation of the constricted capillary vessels after releasing pressure.[4] The capillary perfusion is recovered but remained elevated to the baseline level 2 min after the pressure release [Figs. 4(g) and 4(h)]. For intuitive observation of this hemodynamic, we additionally performed real-time B-mode OCT imaging at the certain location in the nailfold that underwent consecutive pre/post loading. The B-mode imaging speed was 100 fps. OCT structural images and corresponding mOMAG images were obtained from the B-scanned OCT data set and made as a video. Figure 5 shows the representative OCT structural image and corresponding mOMAG image excerpted from the animation video, clearly visualizing time-lapsed change in the structure and the blood perfusion in the nailfold during the pressing.

Moreover, strain maps corresponding to the displacements of the glass slide are visualized in Fig. 6. In Fig. 6(b), distribution of strain is localized at the same site where the capillary occlusion occurred in Fig. 4(b) and enlarged as the displacement is increased from 50 and 200 μm. Since the nailfold is roughly circumferential, its strain magnitude becomes larger around the top surface of the nailfold. In Figs. 6(c) and 6(d), interestingly, the load distributions are caused by the shut-down of blood supply to the peripheral capillaries, leading to subsequent flow cessation in the capillary loops free from the external pressure [see Figs. 4(c) and 4(d)]. At the displacement of $Z = 200$ μm [Fig. 6(e)] where the complete occlusion occurred in Fig. 4(e), the strain distribution is the hottest in color, meaning the strongest pressure distribution over the tissue region of interest. Significant reduction of the strain is apparent right after the lift of the pressure due to immediate recovery of the deformed skin tissue [Fig. 6(f)] where, however, the residual strain is present. After the postpressure, the nailfold deformity is almost restored to the baseline level from the strain maps of Figs. 6(g) and 6(h), respectively. Combining Figs. 4 and 6, one can

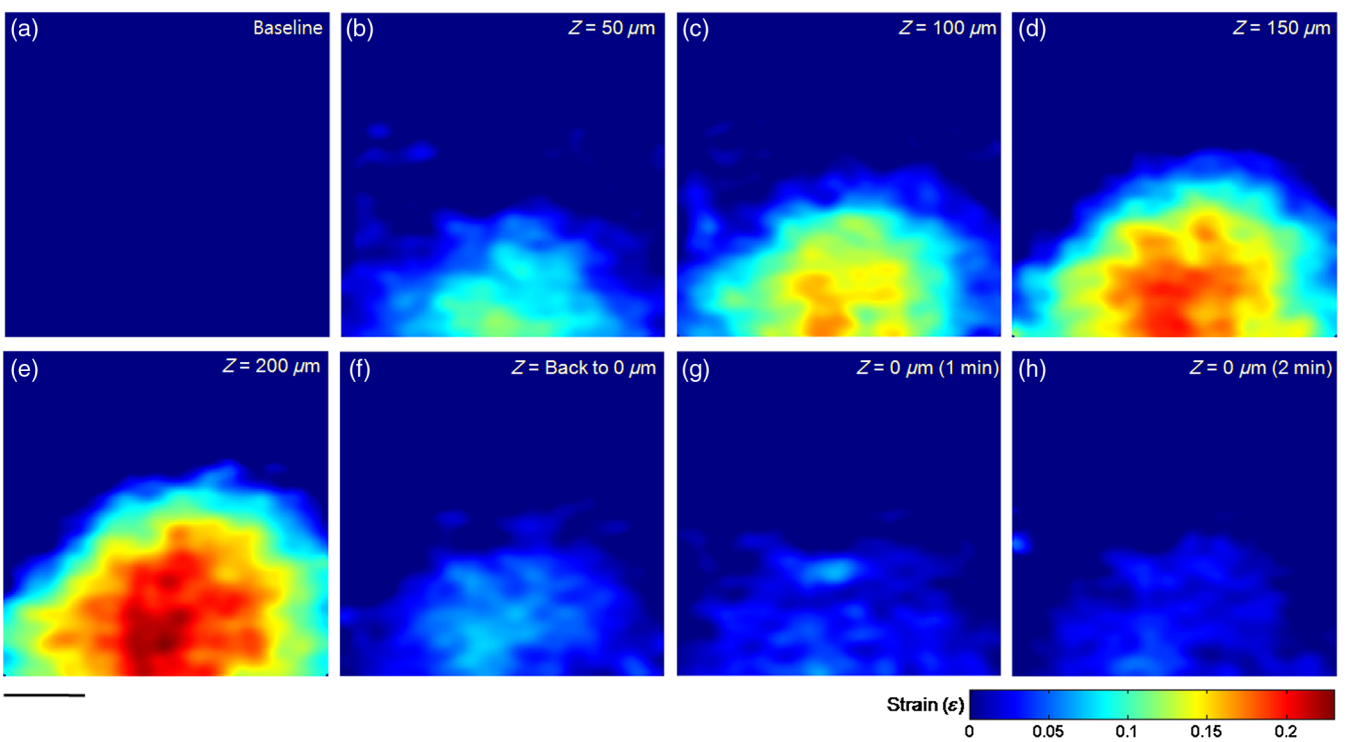

Fig. 6 *En face* strain maps of the nailfold corresponding to the displacements from the initial position of the glass slide in contact to the nailfold surface. (a) Baseline, (b) $Z = 50$ μm, (c) $Z = 100$ μm, (d) $Z = 150$ μm, (e) $Z = 200$ μm, (f) $Z =$ back to 0 μm, (g) $Z = 0$ μm (1 min after pressure releasing), (h) $Z = 0$ μm (2 min after pressure releasing). A scale bar: 500 μm.

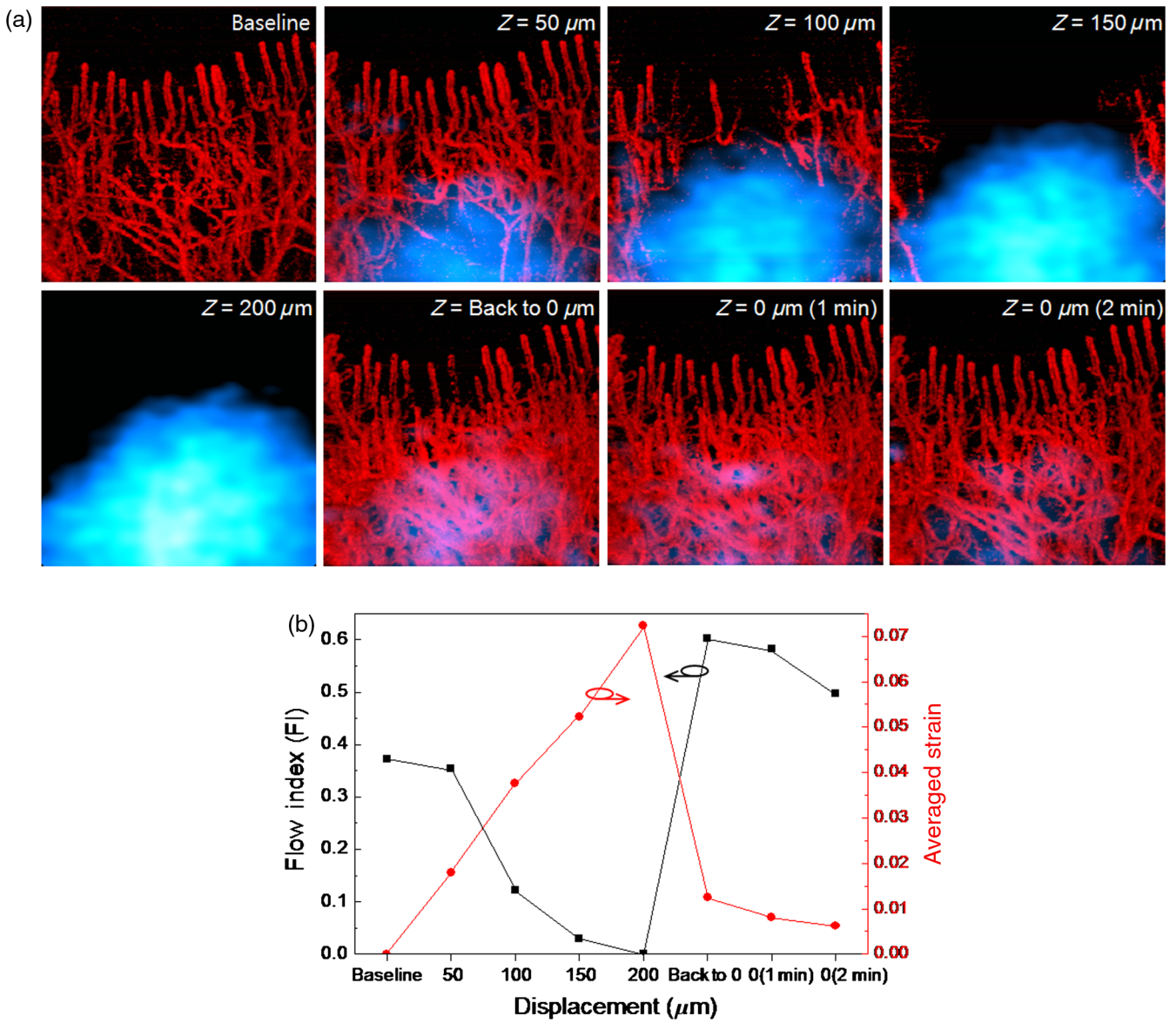

Fig. 7 (a) Overlaid images of the mOMAG angiograms and corresponding strain maps. (b) Flow index versus averaged strain value for each measurement.

conclude that the blood flow response due to applied pressure is correlated very well with the resulted strain maps.

Figure 7(a) shows the overlaid images of the mOMAG angiograms (Fig. 4) and the corresponding strain maps (Fig. 6) for each measurement, showing that the strain distributions are coregistered with the vessel occlusion regions. We calculated the FI and the averaged strain value for each image and the results are graphically represented in Fig. 7(b). In the graph, a progressive decrease in the FI is seen with the linear increase of the strain from 0 to 0.072. Especially, a quick drop of the FI is observed between the strains of 0.018 and 0.037. As the averaged strain reaches 0.072, the FI essentially becomes zero (complete capillary occlusion). After immediate release of the strain (0.012), the FI overshoots up to 0.602, an increase of ~62% above the baseline (0.372), and then slowly decreases by ~34% during a 2-min period of the postreleasing. This pressure-flow curve is quite similar to the results reported in the previous works using the LDI techniques.[3,4,8]

4 Discussion and Conclusion

Traditionally, OCT has been used for structural imaging of skin, eyes, and other internal organs with high-resolution 3-D imaging features, which has assisted in the evaluation of morphological changes in the diseased tissues.[32–34] Recent advances in functional OCT imaging have enabled noninvasive microvascular imaging of the accessible tissues. This vascular measurement is useful for the evaluation of changes in tissue microcirculation in 3-D. We recently developed a new OMAG with mOMAG algorithm capable of obtaining improved microcirculation image in the human skin tissue *in vivo*.[28] In this study, we investigated the ability of our technique to evaluate the vascular perfusion response to the externally applied pressure on the human nailfold. The results showed that the blood perfusion was progressively decreased with the step increase of pressure on the nailfold surface, reaching to minimum (zero) perfusion at the averaged strain of 0.072. When the pressure was released, a dramatic elevation in perfusion (reactive hyperemia) was observed

when compared to the normal state. These perfusion events could be qualitatively and quantitatively identified with the mOMAG angiograms and the corresponding strain maps, providing useful hemodynamic information about the capillaries within the nailfold during pre/postpressure.

In this work, we used the averaged strain of the scanned tissue region as a measure to evaluate the relationship of the microcirculation response to the applied pressure. It is clear that the distribution of tissue strain is dependent on the tissue heterogeneous property and also the unevenness of the tissue surface, making the measured strain highly heterogeneous. It seems that there is a critical value of tissue strain (approximately between 0.1 and 0.12) at which the blood perfusion ceases (see Fig. 7). More study is required to systematically evaluate this critical strain value for useful clinical applications of the proposed OMAG approach.

In addition to the human nailfold, our OMAG method would be also applicable for general skin tissue sites, particularly at the upper and lower body extremities, for example, footsole, where the blood flow response to the external pressure can be considered clinically significant for diagnosis. This envisions a clinical potential that the OCT angiography may quantitatively assess differences in the cutaneous response to postischemic reactive hyperemia between controls and patients with DM or pressure ulcers.[3]

This study using the OCT angiography has some limitations: (1) the actual pressure distribution on the tissue was not determined because of technical difficulty in the current system. Hence, the local strain distribution was experimentally calculated instead of the pressure distribution from a simple strain formula with the assumption that the tissue is uniform, isotropic, and incompressible. In practice, this strain estimation is the source of the error for the measurement of complex, anisotropic skin tissue. The pressure distribution might be inferred from the measured strain map and a known Young's modulus of the human skin tissue.[35] (2) For the quantitative estimation of blood flow within capillaries, this approach using SS-OCT would be challenging due to its unstable phase measurement, making it difficult to calculate the blood flow rate (μl/min) (which is defined as the multiplication of the absolute average velocity of blood and the cross-sectional area of the blood vessel[36]). Use of spectral-domain OCT with high phase stability would be beneficial to quantify the blood flow-pressure relationship. Despitethese limitations, it is worth noting that this work was the first demonstration of OCT angiography to investigate the effect of external pressure on the vascular perfusion of the human skin tissue *in vivo* and its imaging results agreed well with those reported in the previous studies by laser Doppler measurements. The initial finding shows that the OCT angiography is sensitive enough to detect subtle changes in skin perfusion with the applied pressure, indicating that it may be very useful for investigations (both basic and clinical) that require the evaluation of the disturbance in pressure-perfusion relationship that is associated with dysfunction in the tissue microcirculation.

Acknowledgments

This work was supported in part by research grants from the National Institutes of Health (Grant Nos. R01HL093140, R01EB009682, and R01DC010201). The content is solely the responsibility of the authors and does not necessarily represent the official views of grant-giving bodies.

References

1. G. A. Holloway, Jr. et al., "Effects of external pressure loading on human skin blood flow measured by 133Xe clearance," *J. Appl. Physiol.* **40**(4), 597–600 (1976).
2. B. Fromy et al., "Early decrease of skin blood flow in response to locally applied pressure in diabetic subjects," *Diabetes* **51**(4), 1214–1217 (2002).
3. E. Tur, G. Yosipovitch, and Y. Bar-On, "Skin reactive hyperemia in diabetic patients: a study by laser Doppler flowmetry," *Diabetes Care* **14**(11), 958–962 (1991).
4. E. C. Herrman et al., "Skin perfusion responses to surface pressure-induced ischemia: implication for the developing pressure ulcer," *J. Rehabil. Res. Dev.* **36**(2), 109–120 (1999).
5. D. Santos et al., "A review of the effects of external pressure on skin blood flow," *Foot* **13**(4), 185–189 (2003).
6. V. Rajan et al., "Review of methodological developments in laser Doppler flowmetry," *Lasers Med. Sci.* **24**(2), 269–283 (2009).
7. M. Leutenegger et al., "Real-time full field laser Doppler imaging," *Biomed. Opt. Express* **2**(6), 1470–1477 (2011).
8. D. He et al., "Laser Doppler blood flow imaging using a CMOS imaging sensor with on-chip signal processing," *Sensors* **13**(9), 12632–12647 (2013).
9. J. G. Fujimoto et al., "Optical coherence tomography: an emerging technology for biomedical imaging and optical biopsy," *Neoplasia* **2**(1–2), 9–25 (2000).
10. P. H. Tomlins and R. K. Wang, "Theory, developments and applications of optical coherence tomography," *J. Phys. D* **38**(15), 2519–2535 (2005).
11. R. K. Wang et al., "Three dimensional optical angiography," *Opt. Express* **15**(7), 4083–4097 (2007).
12. R. K. Wang and L. An, "Doppler optical micro-angiography for volumetric imaging of vascular perfusion in vivo," *Opt. Express* **17**(11), 8926–8940 (2009).
13. B. J. Vakoc et al., "Three-dimensional microscopy of the tumor microenvironment in vivo using optical frequency domain imaging," *Nat. Med.* **15**(10), 1219–1223 (2009).
14. B. R. Hurley and C. D. Regillo, "Fluorescein angiography: general principles and interpretation," in *Retinal Angiography and Optical Coherence Tomography*, J. Fernando Arevalo, Ed., pp. 27–42, Springer, New York (2009).
15. D. Y. Kim et al., "Noninvasive imaging of the foveal avascular zone with high-speed, phase-variance optical coherence tomography," *Invest. Ophthalmol. Visual Sci.* **53**(1), 85–92 (2012).
16. A. Mariampillai et al., "Speckle variance detection of microvasculature using swept-source optical coherence tomography," *Opt. Lett.* **33**(13), 1530–1532 (2008).
17. J. Enfield, E. Jonathan, and M. Leahy, "*In vivo* imaging of the microcirculation of the volar forearm using correlation mapping optical coherence tomography (cmOCT)," *Biomed. Opt. Express* **2**(5), 1184–1193 (2011).
18. L. An, J. Qin, and R. K. Wang, "Ultrahigh sensitive optical microangiography for in vivo imaging of microcirculations within human skin tissue beds," *Opt. Express* **18**(8), 8220–8228 (2010).
19. R. K. Wang et al., "Depth-resolved imaging of capillary networks in retina and choroid using ultrahigh sensitive optical microangiography," *Opt. Lett.* **35**(9), 1467–1469 (2010).
20. P. Li et al., "*In vivo* microstructural and microvascular imaging of the human corneo-scleral limbus using optical microangiography," *Biomed. Opt. Express* **2**(11), 3109–3118 (2011).
21. Z. Zhi et al., "Noninvasive imaging of retinal morphology and microvasculature in obese mice using optical coherence tomography and optical microangiography," *Invest. Ophthalmol. Visual Sci.* **55**(2), 1024–1030 (2014).
22. Z. Zhi et al., "Impact of intraocular pressure on changes of blood flow in the retina, choroid, and optic nerve head in rats investigated by optical microangiography," *Biomed. Opt. Express* **3**(9), 2220–2233 (2012).
23. R. Reif et al., "Analysis of cross-sectional image filters for evaluating nonaveraged optical microangiography images," *Appl. Opt.* **53**(5), 806–815 (2014).
24. U. Baran, L. Shi, and R. K. Wang, "Capillary blood flow imaging within human finger cuticle using optical microangiography," *J. Biophoton.*, 1–6 (2013).

25. M. Cutolo, W. Grassi, and M. M. Cerinic, "Raynaud's phenomenon and the role of capillaroscopy," *Arthritis Rheum.* **48**(11), 3023–3030 (2003).
26. Y. M. Liew et al., "Reduction of image artifacts in three-dimensional optical coherence tomography of skin in vivo," *J. Biomed. Opt.* **16**(11), 116018 (2011).
27. Y. Jia et al., "Split-spectrum amplitude-decorrelation angiography with optical coherence tomography," *Opt. Express* **20**(4), 4710–4725 (2012).
28. W. J. Choi et al., "Improved microcirculation imaging of human skin in vivo using optical microangiography with a correlation mapping mask," *J. Biomed. Opt.* **19**(3), 036010 (2014).
29. J. Rogowska et al., "Optical coherence tomographic elastography technique for measuring deformation and strain of atherosclerotic tissues," *Heart* **90**(5), 556–562 (2004).
30. X. Yin et al., "Extracting cardiac shapes and motion of the chick embryo heart outflow tract from four-dimensional optical coherence tomography images," *J. Biomed. Opt.* **17**(9), 096005 (2012).
31. J. Qin et al., "Hemodynamic and morphological vasculature response to a burn monitored using a combined dual-wavelength laser speckle and optical microangiography imaging system," *Biomed. Opt. Express* **3**(3), 455–466 (2012).
32. M. Mogensen et al., "Optical coherence tomography for imaging of skin and skin diseases," *Semin. Cutaneous Med. Surg.* **28**(3), 196–202 (2009).
33. Y. Chen et al., "Three-dimensional ultrahigh resolution optical coherence tomography imaging of age-related macular degeneration," *Opt. Express* **17**(5), 4046–4060 (2009).
34. L. P. Hariri et al., "Endoscopic optical coherence tomography and laser-induced fluorescence spectroscopy in a murine colon cancer model," *Laser Surg. Med.* **38**(4), 305–313 (2006).
35. X. Liang and S. A. Boppart, "Biomechanical properties of in vivo human skin from dynamic optical coherence elastography," *IEEE Trans. Biomed. Eng.* **57**(4), 953–959 (2010).
36. Z. Zhi et al., "Volumetric and quantitative imaging of retinal blood flow in rats with optical microangiography," *Biomed. Opt. Express* **2**(3), 579–591 (2011).

Biographies of the authors are not available.